M-ary nonlinear sine chirp spread spectrum for underwater acoustic communication based on virtual time-reversal mirror method

Songzuo Liu[1,2,3], Habib Hussain Zuberi[1,2,3], Yi Lou[1,2,3*], Muhmmad Bilal Farooq[1,2,3], Shahabuddin Shaikh[3] and Waleed Raza[1,2,3]

*Correspondence:
louyi@hrbeu.edu.cn
[1] Acoustic Science
and Technology Laboratory,
Harbin Engineering
University, Harbin 150001,
China
Full list of author information
is available at the end of the
article

Abstract

Linear chirp spread spectrum technique is widely used in underwater acoustic communication because of their resilience to high multipath and Doppler shift. Linear frequency modulated signal requires a high spreading factor to nearly reach orthogonality between two pairs of signals. On the other hand, nonlinear chirp spread spectrum signals can provide orthogonality at a low spreading factor. As a result, it improves spectral efficiency and is more insensitive to Doppler spread than the linear counterpart. To achieve a higher data rate, we propose two variants (half cycle sine and full cycle sine) of the M-ary nonlinear sine chirp spread spectrum technique based on virtual time-reversal mirror (VTRM). The proposed scheme uses different frequency bands to transmit chirp, and VTRM is used to improve the bit error rate due to high multipath. Its superior Doppler sensitivity makes it suitable for underwater acoustic communication. Furthermore, the proposed method uses a simple, low-power bank of matched filters; thus, it reduces the overall system complexity. Simulations are performed in different underwater acoustic channels to verify the robustness of the proposed scheme.

Keywords: Underwater acoustic communication, Nonlinear chirp, Sine chirp, Virtual time-reversal mirror method

1 Introduction

Underwater acoustic communication in the recent past has attracted many researchers because of its application going beyond military uses such as communication between autonomous underwater vehicles (AUVs) for data collection and ocean exploration [1, 2]. Submarine-to-submarine or submarine-to-AUV communication can be achieved through underwater acoustic communication. The underwater acoustic channel is quite challenging compared to traditional terrestrial communication because of the low sound speed of nearly 1500 m/s, high multipath environment, inherit time-varying nature of the ocean, and vehicles' movement adds ups the Doppler effect [3], therefore not only physical layer design is difficult but also designing routing protocol for underwater wireless sensor networks (UWSNs) is also quite challenging [4]. To counter these challenges, researchers have raised many waveforms and modulation schemes. The frequency shift

Liu *et al. J Wireless Com Network*   (2021) 2021:112

Page 2 of 20

keying was used in traditional hydro-acoustic communication. Still, to compensate for multipath interference and high Doppler spread, researchers have raised many spread spectrum techniques, which include Direct Sequences Spread Spectrum (DSSS) and Frequency hop spread spectrum(FHSS) [5]. Linearly modulated signal as a carrier for digital communication was first proposed by the author in [6]. Since then, it is widely studied and implemented in wireless systems [7]. Spread spectrum linear frequency modulation (LFM) signal has gain popularity in low-power and long-range wide area networks (LoRA) [8]. Simultaneously, in UWA communication, this technique is used for decades [9, 10]. The chirp spread spectrum can be categorized into two types: (1) binary orthogonal keying (BOK) and (2) direct modulation (DM). The BOK uses linear upchirp and downchirp to transmit data [11]. In contrast, DM uses chirp signal for spreading purpose along with different modulation schemes [12, 13]. The linear chirp BOK modulation by its nature is resilient to multipath and immune to Doppler shifts [14]; therefore, it is the right candidate for robust hydro-acoustic communication, unlike multi-carrier modulation, which requires high complexity receiver. The main advantage of the LFM signal is that it is easy to implement and have a straightforward matched filter-based receiver. The nonlinear frequency-modulated signals are widely used in radar [15] and sonar applications [16]. Many nonlinear waveforms are available for use as a carrier for UWA communication, such as exponential, log, quadratic, and trigonometric chirps. The authors in [17] have used quadratic and exponential chirp for multiple access users. The result shows that it can reduce multiple access interference under a specific chirp rate. A multi-rate hyperbolic nonlinear chirp spread spectrum proposed in [18] shows better performance than the conventional CDMA system. Many nonlinear chirps have high spreading factor and are non-orthogonal. In contrast, sine chirp signals can be used in many communication and related fields, including ultrasonic positioning [19]. The parameter estimation of sine chirp signal is proposed by the researcher in [20] while, to determine time–frequency bandwidth product authors in [21] proposed discrete sinusoidal frequency modulation transform. Sine chirp as a carrier is implemented for conventional terrestrial communication by the authors in [22], 23. The results show that BOK full period sine chirp is orthogonal at low spreading factor. However, its value of cross-correlation between the pair of complete sine cycle at nonzero time shift is high; as a result, its performance degrades.

The M-ary technique is traditionally used in single-carrier as well as multi-carrier communication to increase the data rate. The M-ary chirp system can be implemented by using various techniques; it can be employed by transmitting in different frequency sub-bands, using different start/stop frequency, also known as pulse positioning, and using different chirp waveforms in the same band. However, in underwater acoustic communication, the bandwidth is limited; therefore, higher-order modulation in different frequency bands cannot be achieved easily. On the other hand, M-ary modulation can be detected using coherent or non-coherent approaches [24]. The authors in [25] employed DPSK and different chirp rates for transmitting M-ary symbols. In contrast, rake receivers were used to improve the overall performance of the system. However, the performance of the system is degraded as multipath increases. M-ary-based cyclic shift keying spread spectrum using VTRM presented in [26] requires a high spreading sequence for a higher data rate. The M-ary linear chirp spread spectrum proposed in

[27] used matched filter to detect chirp signals. However, the linear chirp signal's main problem is that it requires high bandwidth-time (BT) to achieve orthogonality between two chirp signals. As a result, it requires a large bandwidth, which is one of the valuable resources for any communication system, especially in UWA communication, because bandwidth is limited. To increases the data rate of the underwater communication system and to solve the problem of high SF, spectral efficiency, and inter-symbol interference caused by underwater acoustic channels, M-ary Sine Chirp Spread Spectrum (MS-CSS) based on VTRM is proposed in this paper. MS-CSS is a combination of two techniques used in UWA communication. The nonlinear sine upchirp and downchirp is used to represent data bits, and M-ary technique is utilized to achieve a higher bit rate by transmitting at different frequency bands, whereas correlators are used to detect the symbols. In contrast, VTRM implementation helps improve the bit error rate caused by the multipath environment.

The rest of the paper is organized as follows: Sect. 2 introduces the analysis of linear and nonlinear chirp signals. Section 3 presents the chirp spread spectrum concept using the M-ary technique, whereas the system model of the M-ary sine chirp spread spectrum is given in Sect. 4. The channel estimation using matching pursuit and virtual time-reversal mirror methods is provided in Sect. 5 and Sect. 6, respectively. Section 7 validates the proposed scheme's simulation results and Sect. 8 finally concludes the research article.

2 Analysis of linear and nonlinear chirp signal

2.1 Linear chirp signal

In traditional chirp, signal frequency increases linearly (upchirp) and decreases (downchirp) over a given time period. The LFM signal can be expressed as
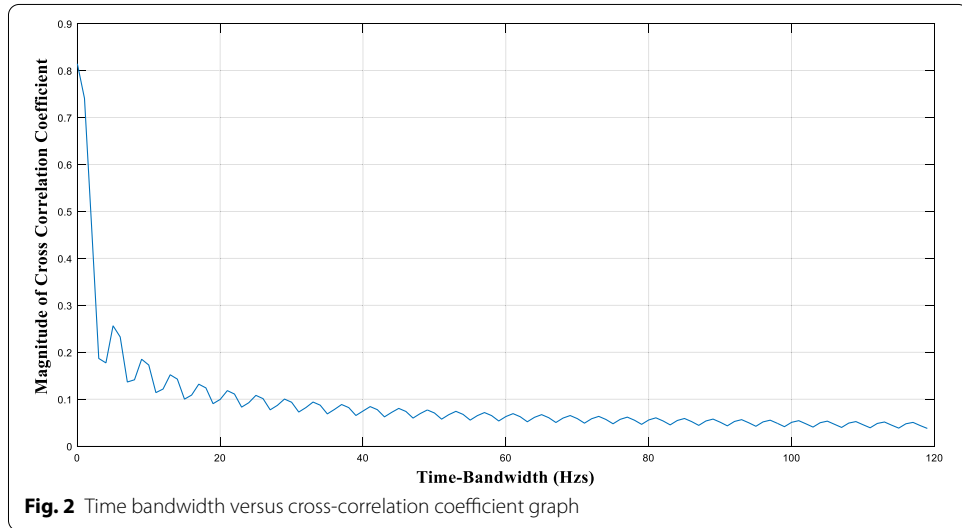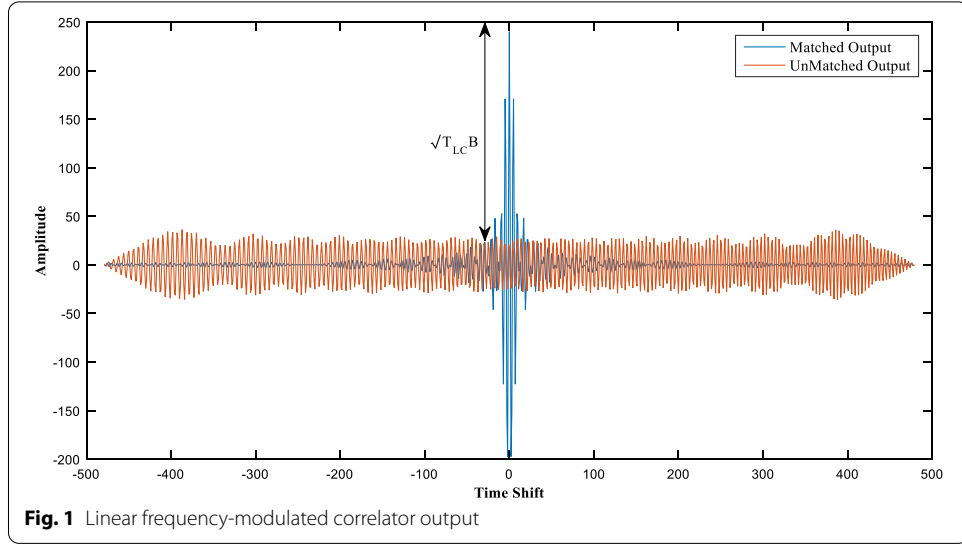
$$
\begin{cases}
\text{Up Chirp}: & c_0(t) = A\cos(2\pi f_o t + \pi\mu t^2) - \dfrac{T_{LC}}{2} \le t \le \dfrac{T_{LC}}{2} \\
\text{Down Chirp}: & c_1(t) = A\cos(2\pi f_o t - \pi\mu t^2) - \dfrac{T_{LC}}{2} \le t \le \dfrac{T_{LC}}{2}
\end{cases}
\tag{1}
$$

where A is the amplitude of the chirp, f_o is the starting frequency, T_{LC} is the chirp duration, and μ is the frequency sweep rate and can be defined as $\mu = B/T_{LC}$ where B is the bandwidth and can be defined as $B = f_{\text{final}} - f_{\text{initial}}$. When the bit "0" is to be sent, the function $c_0(t)$ that is upchirp is transmitted, and when bit "1" is to be sent, function $c_1(t)$ downchirp is transmitted. The matched filter-based receiver is used for detection. The expression for the autocorrelation and cross-correlation in [28] and it can be given as,

$$
r_{c_0 c_0}(\tau) = \sqrt{\mu}\,\frac{\sin[\pi\mu t(T_{LC} - |\tau|)]}{2\pi\mu\tau}\cos(2\pi f_o \tau) - \frac{T_{LC}}{2} \le \tau \le \frac{T_{LC}}{2}
\tag{2}
$$

$$
r_{c_0 c1}(\tau) = \frac{\cos(2\pi f_o \tau)}{\sqrt{T_{LC}B}}\left[C\left(\frac{\pi}{2}\left(\sqrt{T_{LC}B} - |\tau|\sqrt{\mu}\right)^2\right) + jS\left(\frac{\pi}{2}\left(\sqrt{T_{LC}B} - |\tau|\sqrt{\mu}\right)^2\right)\right]
\tag{3}
$$

where $C(x)$ and $S(x)$ are defined as the Fresnel function. Figure 1 shows that the output function of a matched filter has most of its energy existing from $-1/B \le \tau \le 1/B$ of period, and the peak of the matched filter is amplified up to $\sqrt{T_{LC}B}$. This pulse

Liu *et al. J Wireless Com Network*   (2021) 2021:112

Page 4 of 20

Fig. 1 Linear frequency-modulated correlator output

Fig. 2 Time bandwidth versus cross-correlation coefficient graph

compression property of LFM makes it resilient to multipath and Doppler shifts. The cross-correlation coefficient of LFM is defined by

$$|\rho_l| = \frac{1}{\sqrt{T_{LC}B}} \sqrt{\left(\int_0^{\sqrt{T_{LC}B}} \cos\left(\frac{\pi v^2}{2}\mathrm{d}v\right)\right)^2 + \left(\int_0^{\sqrt{T_{LC}B}} \sin\left(\frac{\pi v^2}{2}\mathrm{d}v\right)\right)^2} \qquad (4)$$

Figure 2 shows that the cross-correlation coefficient ρ_l depends upon the product of time period of linear chirp T_{LC}, and the bandwidth B of the chirp signal. As $T_{LC}B$ increases, ρ_l decreases, but it never reaches 0, even if the $T_{LC}B$ is equal to 100. Therefore, linear chirps are not entirely orthogonal, even at a high $T_{LC}B$ value and can be considered quasi-orthogonal [29].

Liu *et al. J Wireless Com Network*   (2021) 2021:112

Page 5 of 20

2.2 Nonlinear chirp signal analysis

There are many candidates of nonlinear chirps as a carrier, but one of the preferable contenders for UWA communication can be sine chirp because of its orthogonality between the pair of chirp under certain conditions. The sine chirp can be mathematically written as

$$
\begin{cases}
\text{Up:} \quad c_{s0}(t) = A \cos\left[2\pi f_o t + \dfrac{BT_S}{\eta} \cos\left(\pi\eta\dfrac{t}{T_s}\right)\right] \quad -\dfrac{T_S}{2} \le t \le \dfrac{T_S}{2} \\[3mm]
\text{Down:} \quad c_{s1}(t) = A \cos\left[2\pi f_o t - \dfrac{BT_S}{\eta} \cos\left(\pi\eta\dfrac{t}{T_s}\right)\right] \quad -\dfrac{T_S}{2} \le t \le \dfrac{T_S}{2}
\end{cases}
\tag{5}
$$

where T_S is the duration of the sine chirp, and η represents the number of cycles. For example, if η is set to "1" in Eq. (5), half-cycle sine chirp is obtained, whereas if η is set to "2" in Eq. (5), full-cycle sine chirp is obtained. The autocorrelation property of the sine chirp is similar to the linear chirp signal and can be expressed using the equation.

$$
\begin{aligned}
r_{c_{s1}c_{s1}}(\tau) = {}&\left(1 - \frac{|\tau|}{T_s}\right) \sum_{n=-\infty}^{n=+\infty} \left\{(-1)^n J_{2n}(k_{s_1}^m) \sin c[(\omega_L + 2n\theta)(T_s - |\tau|)]\right\} \\
&+ \left(1 - \frac{|\tau|}{T_s}\right) \cos(\omega_L \tau) J_o(k_{s_2}^m) \\
&+ 2\left(1 - \frac{|\tau|}{T_s}\right) \cos(\omega_L \tau) \sum_{n=1}^{\infty} \left\{J_{2n}(k_{s_2}^m) \sin c[(2n\theta)(T_s - |\tau|)]\right\}
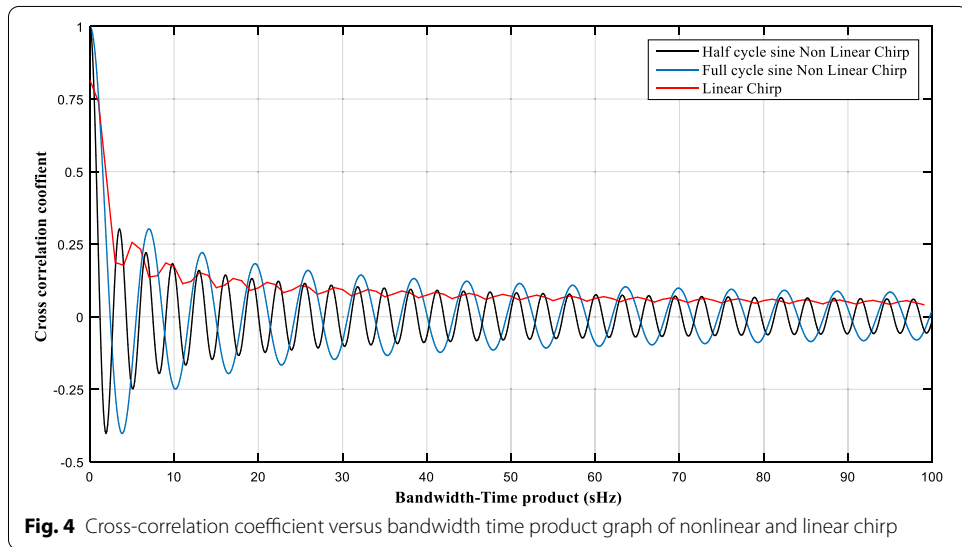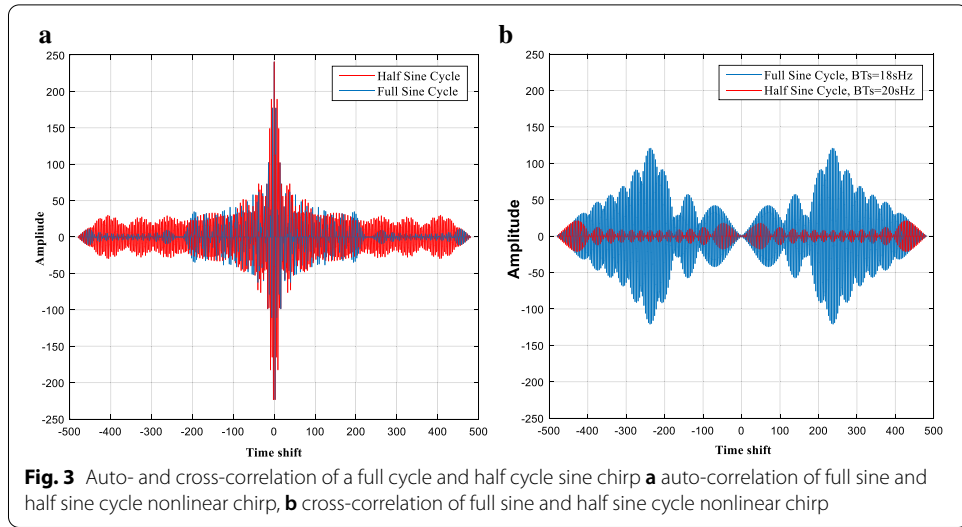\end{aligned}
\tag{6}
$$

where $\theta = \frac{\pi\eta}{2T_s}$, $k_{s_1}^m = \frac{2BT_s}{\eta} \cos\left(\frac{\pi\eta}{2T_s}\tau\right)$, $k_{s_2}^m = \frac{2BT_s}{\eta} \sin\left(\frac{\pi\eta}{2T_s}\tau\right)$ and J_{2n} is the first kind Bessel function. In Eq. (6), the first and third terms have a negligible effect on the autocorrelation coefficient. Hence Eq. (6) is written as

$$
r_{c_{s1}c_{s1}}(\tau) \approx \left(1 - \frac{|\tau|}{T_s}\right) \cos(\omega_L \tau) J_o\left(\frac{2BT_s}{\eta} \sin\left(\frac{\pi\eta}{2T_s}\tau\right)\right)
\tag{7}
$$

The following equation gives the cross-correlation coefficient of pair of sine chirp
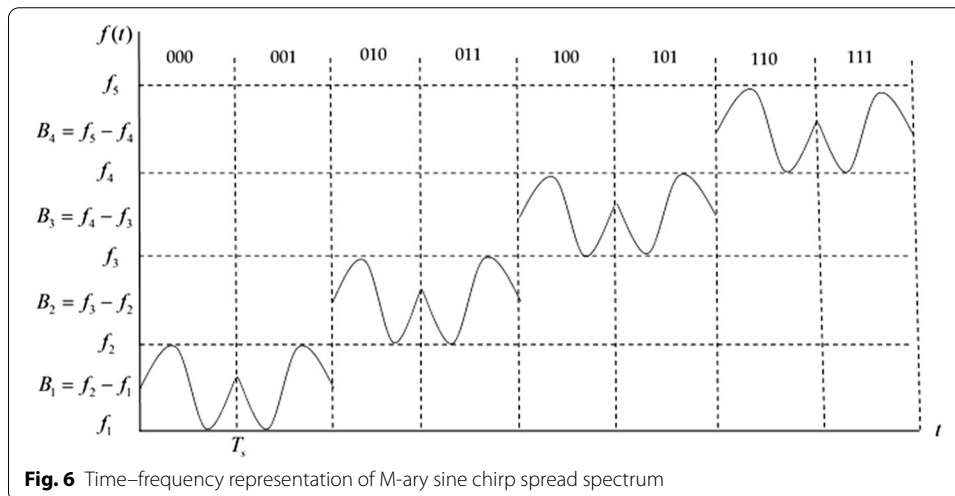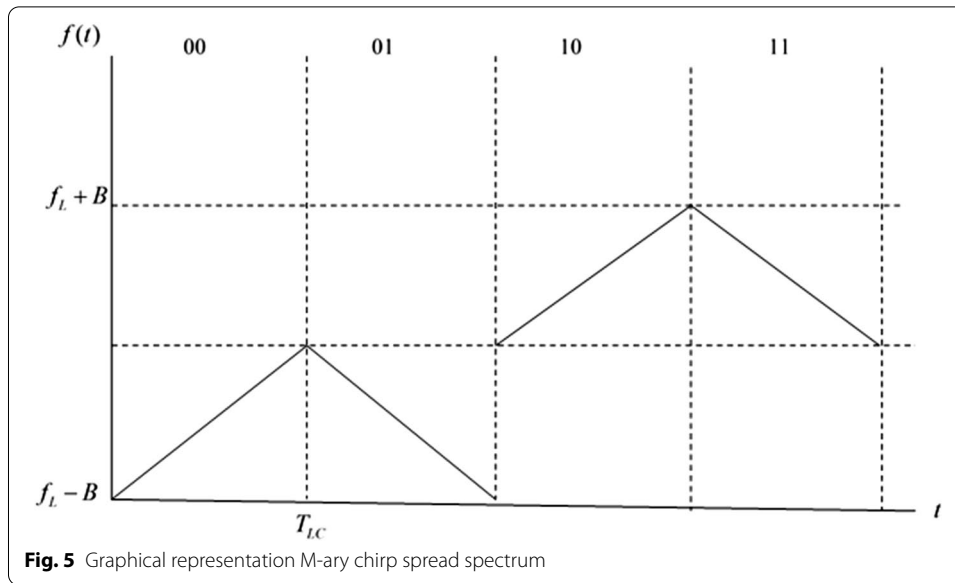
$$
\begin{aligned}
\rho_s(\tau) = {}&\left(1 - \frac{|\tau|}{T_s}\right) \sum_{n=-\infty}^{n=+\infty} \left\{(-1)^n J_{2n}(k_{s_1}^u) \sin c[(\omega_L + 2n\theta)(T_s - |\tau|)]\right\} \\
&+ \left(1 - \frac{|\tau|}{T_s}\right) \cos(\omega_L \tau) J_o(k_{s_2}^u) \\
&+ 2\left(1 - \frac{|\tau|}{T_s}\right) \cos(\omega_L \tau) \sum_{n=1}^{\infty} \left\{J_{2n}(k_{s_2}^u) \sin c[(2n\theta)(T_s - |\tau|)]\right\} \\
&- 2\left(1 - \frac{|\tau|}{T_s}\right) \sin(\omega_L \tau) \sum_{n=0}^{\infty} \left\{J_{2n+1}(k_{s_2}^u) \sin c[(2n\theta)(T_s - |\tau|)]\right\}
\end{aligned}
\tag{8}
$$

where $\theta = \frac{\pi\eta}{2T_s}$, $k_{s_1}^m = \frac{2BT_s}{\eta} \cos\left(\frac{\pi\eta}{2T_s}\tau\right)$, $k_{s_2}^m = \frac{2BT_s}{\eta} \sin\left(\frac{\pi\eta}{2T_s}\tau\right)$ and J_n is the first kind Bessel function. The cross-correlation coefficient at time shift $\tau = 0$ can be simplified as in [30] and given by the equation below.

Liu *et al. J Wireless Com Network*   (2021) 2021:112

Page 6 of 20

Fig. 3 Auto- and cross-correlation of a full cycle and half cycle sine chirp **a** auto-correlation of full sine and half sine cycle nonlinear chirp, **b** cross-correlation of full sine and half sine cycle nonlinear chirp

Fig. 4 Cross-correlation coefficient versus bandwidth time product graph of nonlinear and linear chirp

$$\rho_s(0) \approx J_0\left(\frac{2T_sB}{\eta}\right) \tag{9}$$

Figure 4 shows that the cross-correlation coefficient and bandwidth time product of nonlinear sine chirps (half and full cycle) are periodically zero; hence, they are entirely orthogonal at the specific condition. For example, the half-sine period has a cross-correlation coefficient zero at various periodic bandwidth–time product points, including 4.4 sHz, 9 sHz, and 20 sHz, while the full sine period has zero cross-correlation coefficient at bandwidth–time 5.5 sHz, 8.65 sHz, and 18 sHz. In contrast, the LFM signal never reaches zero. Figure 3a shows that the autocorrelation between the pair of one complete sine cycle and the half-sine cycle is similar to the linear chirp. Still, side lobes of both the nonlinear chirps are greater than linear counterparts, which can be reduced using any side lobe reduction scheme. Figure 3b verifies the relationship between the

Fig. 5 Graphical representation M-ary chirp spread spectrum

Fig. 6 Time–frequency representation of M-ary sine chirp spread spectrum

cross-correlation coefficient and bandwidth time product of nonlinear chirps. The cross-correlation between the pair to full and half-period sine chirp at 18sHz and 20sHz in Fig. 3b shows that at time shift ($\tau = 0$) the value of cross-correlation is zero for both cycles. However, the full period sine chirp has a large value at non zero time shift, resulting in false detection in the UWA dispersive channel. As a result, the overall performance of the system can be affected. Similar results can be obtained for BT's different values; as the value of BT is decreased, the side lobe of auto-correlation increases for both linear and nonlinear chirp signals (Fig. 4).

3 M-ary chirp spread spectrum

M-ary chirp spread spectrum can be implemented by transmitting upchirp and downchirp in two different frequency bands, as shown in Fig. 5. The main issue with linear chirp is that it requires high BT products to achieve acceptable performance. As

Fig. 7 Block diagram of 8-ary sine chirp spread spectrum communication system
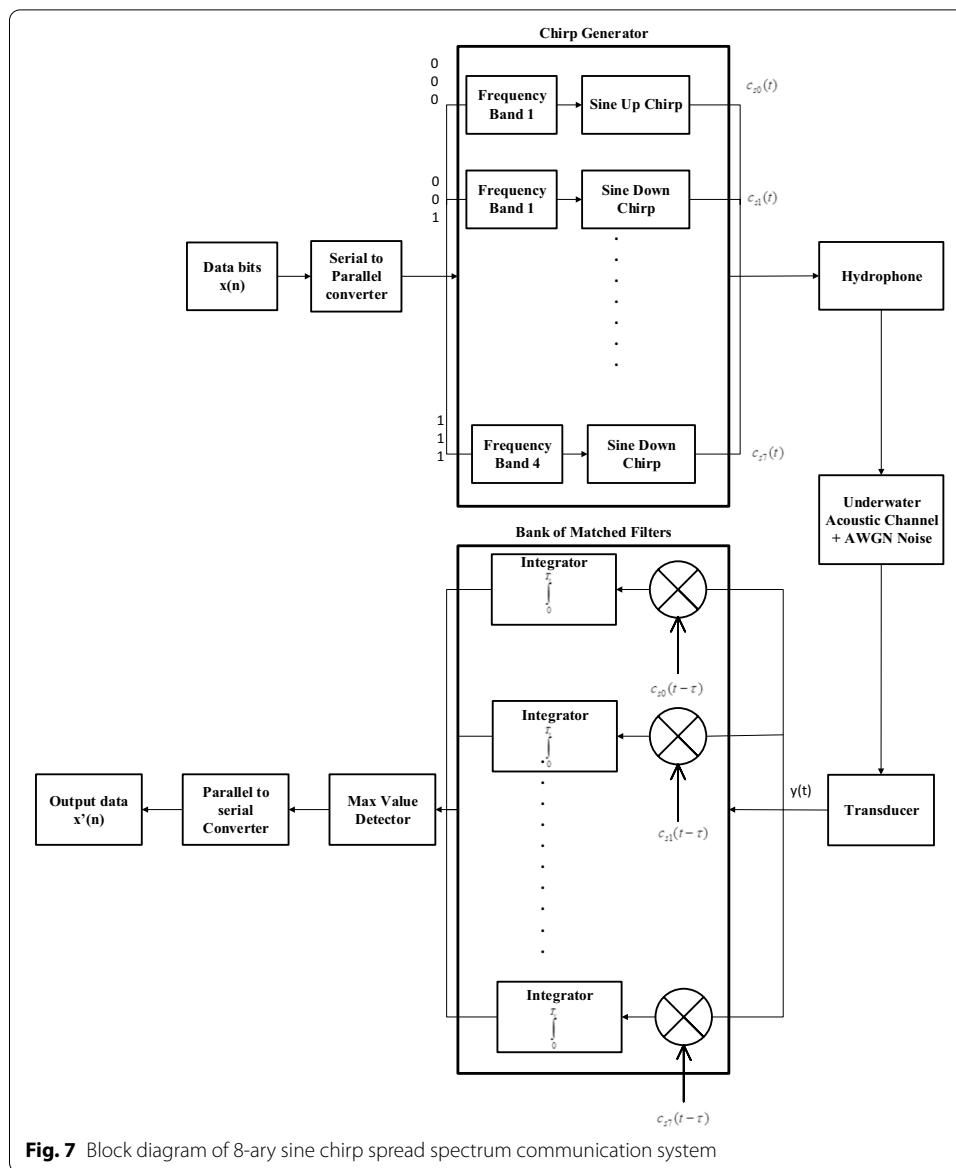
the number of chirps are increased to increase the data rate, the system's overall performance is worsening. The sine chirp is used in this paper, for which the pair of chirp is orthogonal at low SF. In Fig. 6, the time–frequency graph of 8-ary sine chirp at four different frequency bands is shown. When the symbol to be transmitted is "000", the sine chirp in the first frequency band with a positive gradient is transmitted similarly. If "001" is transmitted, the frequency band is the same but having a negative gradient. As a result, there is a 180 phase shift in sine chirp, as shown in Fig. 6. For the next two symbols, the frequency band ranges from f_2 to, f_3 and upchirp and downchirp is transmitted

Liu *et al. J Wireless Com Network*   (2021) 2021:112

Page 9 of 20

according to the symbol assign against it. Similarly, the last two symbols are assigned upchirp and downchirp from frequency f_4 to f_5. Similarly, the half-sine cycle can also be represented using a time–frequency graph.

4 System model of MS-CSS

The block diagram of the M-ary sine chirp spread spectrum is shown in Fig. 7. First, the stream of serial data bits $x(n)$ is converted from serial to parallel, then chirp is generated by the chirp generator according to the given symbol; for example, if the symbol to be transmitted is "000", then upchirp $c_{s0}(t)$ is generated in the frequency band 1 as shown in Fig. 7, then it is pass through the hydrophone for transmitting it through an underwater acoustic channel in the presence of Additive White Gaussian Noise (AWGN). The transmit signal is received by the transducer and passed through the bank of matched filters. The matched filter works on the principle of correlation. The received signal $y(t)$ is multiplied with a time-shifted version of the initially generated chirp $c_{s0}(t - \tau)$(in this case) and integrated over the chirp period T_s. The matched signal gives maximum output while all other unmatched output has low values. As a result, the maximum value detector determines the given chirp signal, and the corresponding symbol is mapped against it. Finally, the output data is received by converting the given symbols from parallel to serial.

5 Channel estimation

The channel estimation is one of the requisite components of VTRM-based systems. Its performance is highly dependent on how accurately the channel is estimated. The sparse nature of the UWA channel results in a considerable delay spread with minimal nonzero values. Compressed sensing algorithms are widely used to solve the problem of sparsity [31]. In many underwater acoustic communication systems, compressed sensing algorithms are used. In [32], a compressed sensing algorithm and equalization are used to evaluate orthogonal signal division multiplexing performance. In contrast, matching pursuit helps resolve the problem of sparse channel estimation. It is widely used due to its robustness and computational efficiency [33]. Matching pursuit along with VTRM used in [26, 34], 35 proves to be very useful. The channel is estimated by sending a training signal through a sparse UWA channel. The training signal received can be given by the following equation

$$y(n) = \sum_{n=0}^{L-1} x(t - n) * h(n) + v(n) \tag{10}$$

Let $y(n)$ is the received training signal and l its length, where the number of channel taps. The above equation can be rewritten as

Liu *et al. J Wireless Com Network*   (2021) 2021:112

Page 10 of 20

$$\underbrace{\begin{bmatrix} y(0) \\ y(1) \\ \vdots \\ y(l-2) \\ y(l+L-1) \end{bmatrix}}_{Y} = \underbrace{\begin{bmatrix} x(0) & 0 & \cdots & 0 \\ x(1) & x(0) & \cdots & 0 \\ \vdots & \vdots & \cdots & 0 \\ 0 & 0 & \ddots & x(l-1) \\ 0 & 0 & \cdots & x(l) \end{bmatrix}}_{X} * \underbrace{\begin{bmatrix} h(0) \\ h(1) \\ \vdots \\ h(L-2) \\ h(L-1) \end{bmatrix}}_{h} + \underbrace{\begin{bmatrix} v(0) \\ v(1) \\ \vdots \\ v(L+l-2) \\ v(L+l-1) \end{bmatrix}}_{V}$$

(11)

It can be concluded from the above equation that most of the channel taps are either zero or have minimal values.

The iteration process estimates the channel until the given threshold is achieved. Initially, the received signal Y is considered as a residual Υ_0 and Υ_0 is appropriately matched with the column of X, which is denoted by x_1. If the threshold is not achieved, the irritation continues. At mth iteration, the residual Υ_{m-1} for which the X has the maximal rank-one projection can be expressed as x_m and it is given by the following equation

$$x_m = \arg\max_{k \notin I_{m-1}} \frac{\left| X_k^H \Upsilon_{m-1} \right|}{\|X_k\|^2}$$

(12)

X_k contains the column of X and the superscript H is Hermitian Transpose. The value of $\hat{h}_m$ which can be defined as the components h associated with X_k can be computed as

$$\hat{h}_m = \frac{\left| X_{x_m}^H \Upsilon_{m-1} \right|}{\left\| X_{x_m} \right\|^2}$$

(13)

Finally, the residual vector can be calculated as

$$\Upsilon_m = \Upsilon_{m-1} - \hat{h}_m X_{x_m}$$

(14)

6 Virtual time-reversal mirror method

The virtual time-reversal mirror method is widely used for equalization in many types of communication channels, including underwater acoustic communication channel [36]. VTRM-based equalization had proven to be effective in underwater acoustic single

Fig. 8 VTRM-based system design
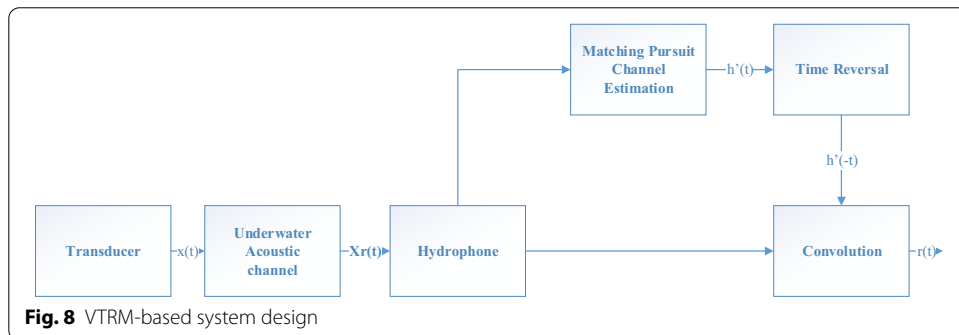
carrier chirp spread communication. The authors in [37] proposed orthogonal chirp carrier, and to mitigate the effect of inters symbol interference VTRM is used. Moreover, VTRM proves to be useful in multiuser chirp spread spectrum communication proposed in [38]. Furthermore, VTRM is also used in time-varying underwater acoustic communication channel [39, 40].

The idea behind the working principle of the VTRM technique is to estimate the channel impulse response by processing the received training signal. The authors in [41] showed that the performance of VTRM is dependent on the use of appropriate training signals and the duration of the time window. The VTRM system design is shown in Fig. 8; first, the estimated channel impulse response $h^{'}(t)$ is time-reversed $h^{'}(-t)$, and then it is convolved with the received signal [42].

Let $x_r(t)$ be the transmit signal passed through the UWA channel can be given as

$$x_r(t) = x(t) \otimes h(t) + n(t) \tag{15}$$

Then after virtual time reversal, the received signal can be expressed as

$$r(t) = x_r(t) \otimes h^{'}(-t) \tag{16}$$

$$r(t) = \left\{ x(t) \otimes h(t) + n(t) \right\} \otimes h^{'}(-t) \tag{17}$$

$$r(t) = x(t) \otimes \left[h(t) \otimes h^{'}(-t) \right] + n(t) \otimes h^{'}(-t) \tag{18}$$

The above equation $h(t) \otimes h^{'}(-t)$ is VTRM based on equalized channel. It is a concurrence between the real channel impulse response and estimated channel impulse response. If the channel is estimated precisely, the direct path's energy concentration is much greater than the other reflected paths in the matched channel. As a result, it not only reduces inter-symbol interference but also improves the SNR.

7 Results and discussion

7.1 Simulation using BELL HOP ray tracing algorithm

The parameters used for the simulation are shown in Table 1. The simulation setup of the UWA channel generated using the BELLHOP ray tracing algorithm is shown in Fig. 9. The actual impulse response of a channel and estimated channel response when the distance between transmitter and receiver is 1 km is shown in Fig. 10.

The simulation results in Fig. 11 depict that when the chirp period is 10 ms and Spread factor is 9sHz for half cycle sine (HCS) chirp and LFM, whereas 8.65sHz for full cycle sine (FCS) chirp without channel estimation and VTRM, the BER of HCS chirp is zero after -4 dBs. For the case of FCS chirp and LFM, the BER is zero after -2 dB. The UWA channel exhibits high multipath. Consequently, the system's overall performance is affected, but using VTRM improves the bit error rate. As shown in Fig. 11, using the VTRM method, all three types of Chirps' performance is improved while HCS Chirp outperforms the other two types. To investigate further, the BT was decreased from 9sHz to 4.4sHz for HCS chirp and LFM, while for FCS chirp, it was decreased from 8.65sHz to 5.5sHz as at the mentioned values, nonlinear chirps are orthogonal. The simulation

Table 1 Simulation parameters

Type of chirp	Time period of chirp (ms)	Frequency bands (Hz)	Time bandwidth product BT_s (sHz)	Depth of source (m)	Depth of receiver (m)	Distance between Tx and Rx (km)	Data rate (bps)
Half cycle sine chirp	10 ms	5000–4100 8000–7100 12,000–11,100 16,000–15,100	9 sHz	40 m	30 m	1 km	300 bps
Half cycle sine chirp	10 ms	5000–4560 8000–7560 12,000–11,560 16,000–15,560	4.4 sHz	40 m	30 m	1 km	300 bps
Half cycle sine chirp	5 ms	5000–3200 8000–6200 12,000–10,200 16,000–14,200	9 sHz	40 m	30 m	1 km	600 bps
Half cycle sine chirp	5 ms	5000–4120 8000–7120 12,000–11,120 16,000–15,120	4.4 sHz	40 m	30 m	1 km	600 bps
Full cycle Sine chirp	10 ms	5000–4135 8000–7135 12,000–11,135 16,000–15,135	8.65 sHz	40 m	30 m	1 km	300 bps
Full cycle sine chirp	10 ms	5000–4450 8000–7450 12,000–11,450 16,000–15,450	5.5 sHz	40 m	30 m	1 km	300 bps
Full cycle sine chirp	5 ms	5000–3270 8000–6270 12,000–10,270 16,000–14,270	8.65 sHz	40 m	30 m	1 km	600 bps
Full cycle sine chirp	5 ms	5000–3900 8000–6900 12,000–10,900 16,000–14,900	5.5 sHz	40 m	30 m	1 km	600 bps
Linear chirp	10 ms	5000–4100 8000–7100 12,000–11,100 16,000–15,100	9 sHz	40 m	30 m	1 km	300 bps
Linear chirp	10 ms	5000–4560 8000–7560 12,000–11,560 16,000–15,560	4.4 sHz	40 m	30 m	1 km	300 bps

Table 1 (continued)

Type of chirp	Time period of chirp (ms)	Frequency bands (Hz)	Time bandwidth product BT_s (sHz)	Depth of source (m)	Depth of receiver (m)	Distance between Tx and Rx (km)	Data rate (bps)
Linear chirp	5 ms	5000–3200 8000–6200 12,000– 10,200 16,000– 14,200	9 sHz	40 m	30 m	1 km	600 bps
Linear chirp	5 ms	5000–4120 8000–7120 12,000– 11,120 16,000– 15,120	4.4 sHz	40 m	30 m	1 km	600 bps
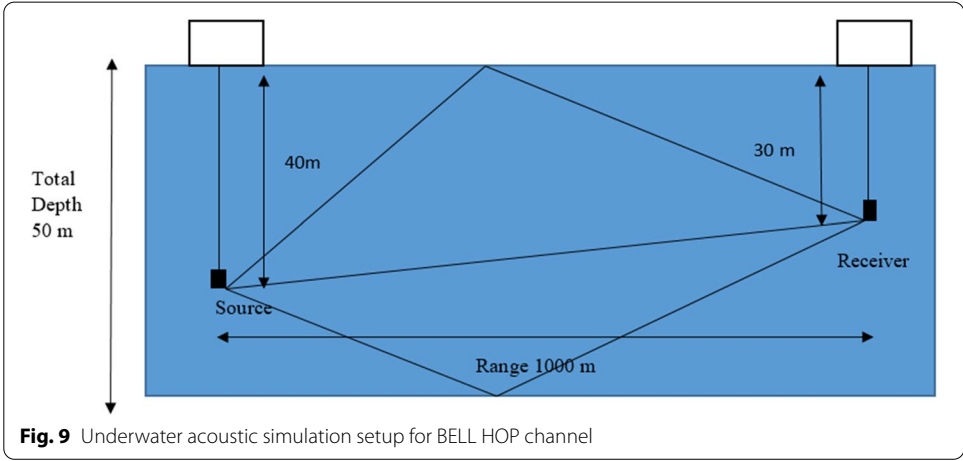
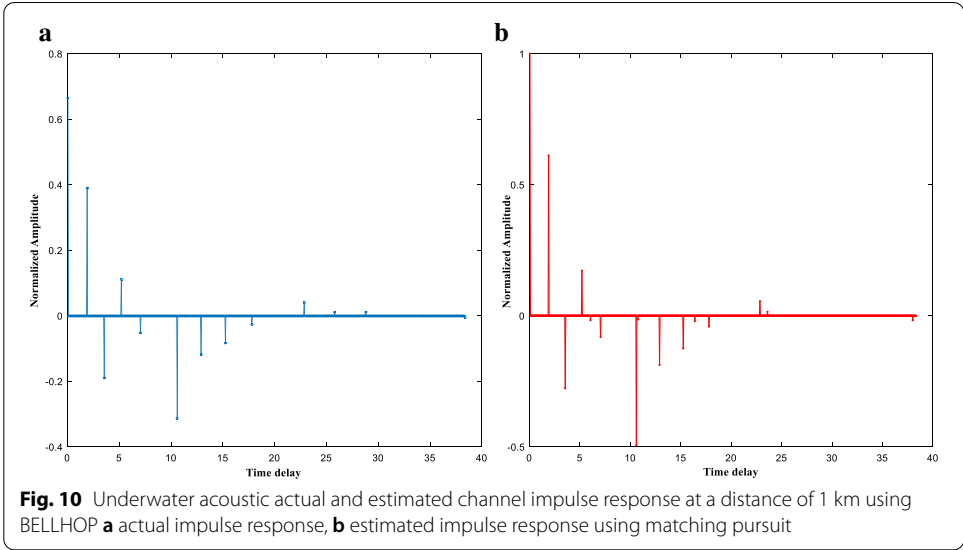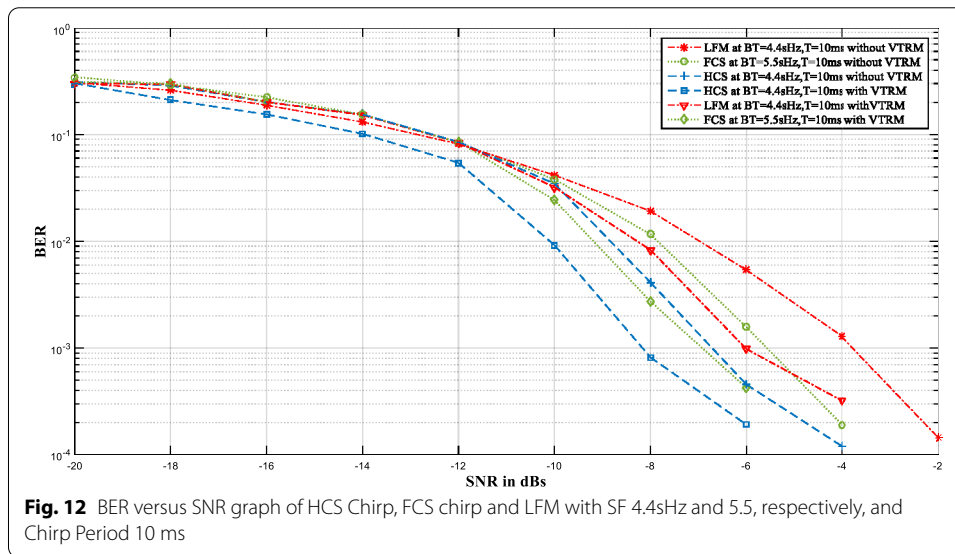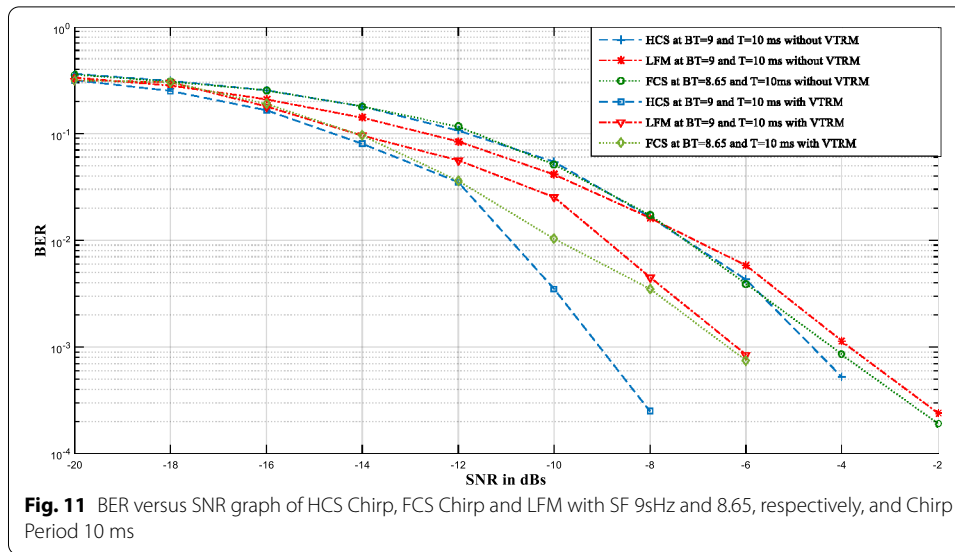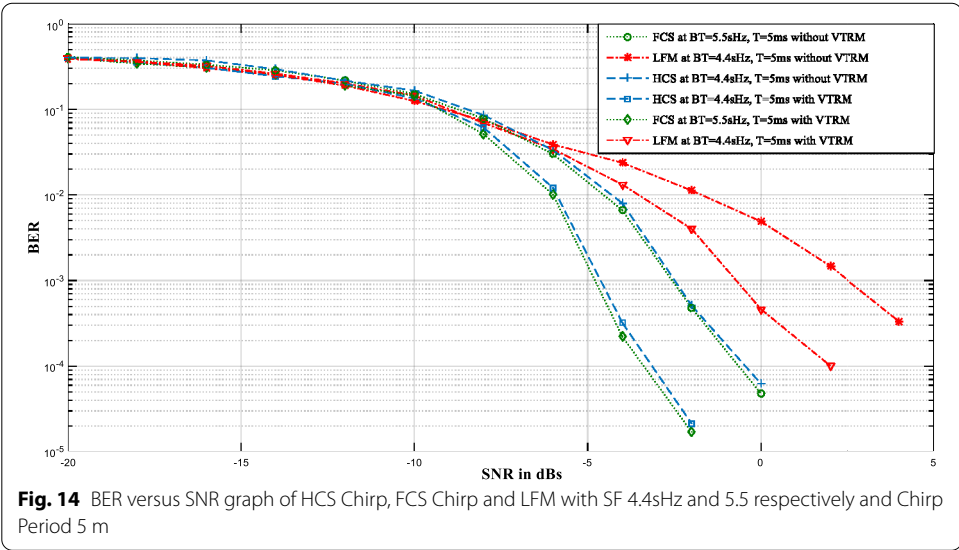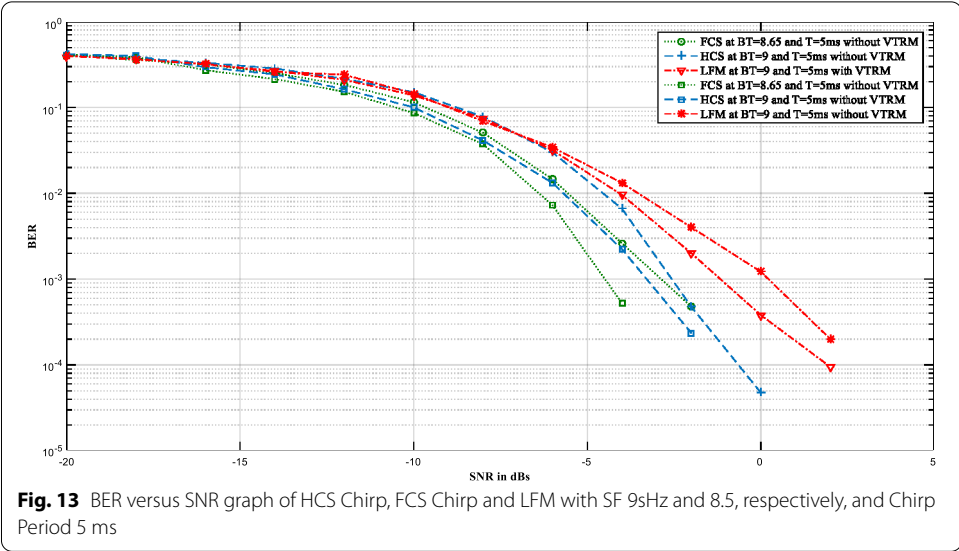**Fig. 9** Underwater acoustic simulation setup for BELL HOP channel

Fig. 10 Underwater acoustic actual and estimated channel impulse response at a distance of 1 km using BELLHOP **a** actual impulse response, **b** estimated impulse response using matching pursuit

Fig. 11 BER versus SNR graph of HCS Chirp, FCS Chirp and LFM with SF 9sHz and 8.65, respectively, and Chirp Period 10 ms

Fig. 12 BER versus SNR graph of HCS Chirp, FCS chirp and LFM with SF 4.4sHz and 5.5, respectively, and Chirp Period 10 ms

results shown in Fig. 12 indicate that as the SF is decreased, linear chirp performance deteriorates compared to nonlinear chirp.

To increase the bit rate, the chirp period was decreased from 10 to 5 ms. The result shown in Fig. 13 indicates that the performance of the nonlinear sine full cycle is better than the other two types. In contrast, at low SF the full cycle and half-cycle have similar performance but outperform the linear chirp, as illustrated in Fig. 14. The simulation results validate that the MS-CSS solves the problem of increasing the information rate at low spreading factor and improving the system's overall performance influenced by the high multipath due to underwater acoustic channel by using the VTRM technique.
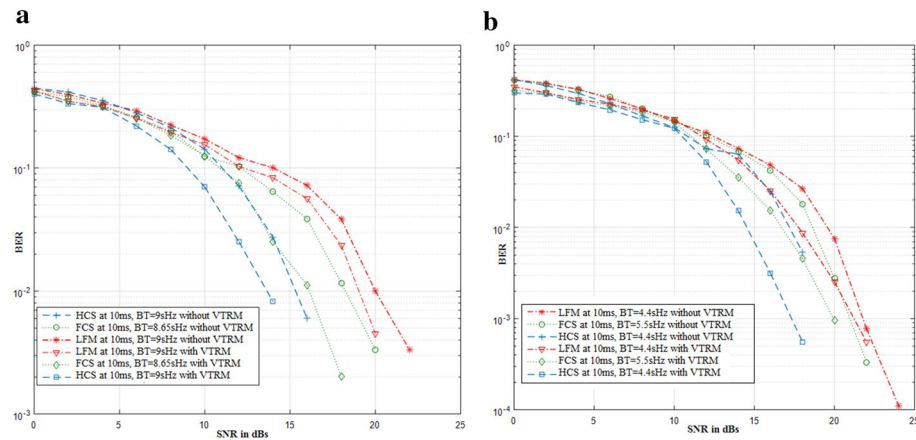
Fig. 13 BER versus SNR graph of HCS Chirp, FCS Chirp and LFM with SF 9sHz and 8.5, respectively, and Chirp Period 5 ms

Fig. 14 BER versus SNR graph of HCS Chirp, FCS Chirp and LFM with SF 4.4sHz and 5.5 respectively and Chirp Period 5 m

Table 2 Watermark benchmark NOF1 simulation channel parameters as given in [43]

Parameters	Value
Channel	NOF1
Water depth	10 m
Transmitter	Bottom
Receiver	Bottom
Range	750 m
Frequency band	10–18 kHz
Doppler coverage	7.8 Hz
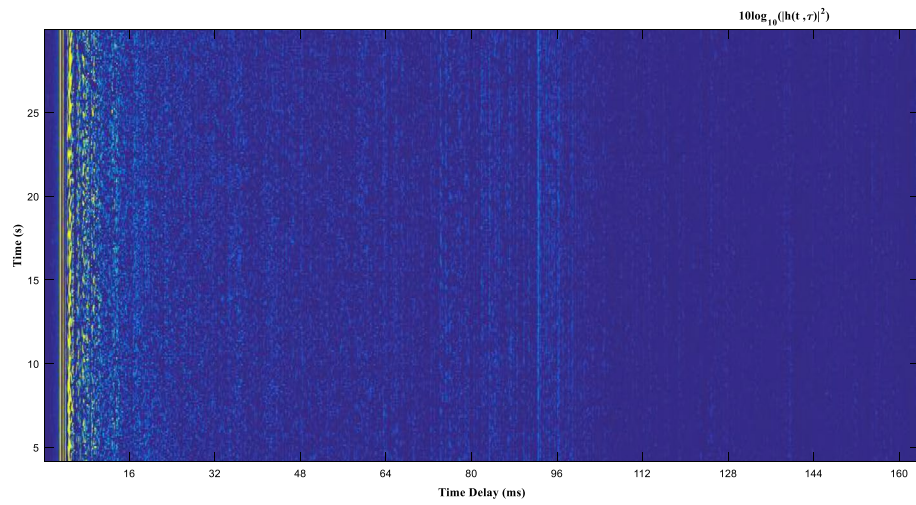
Fig. 15 Time-varying channel impulse response of a NOF1 watermark channel

Fig. 16 BER versus SNR graph proposed system in watermark channel **a** BER versus SNR graph of HCS Chirp, FCS Chirp and LFM with SF 9sHz and 8.65, respectively, and Chirp Period 10 ms, **b** BER versus SNR

7.2 Simulation using watermark reply channel

The watermark replay channel is a time-varying UWA channel; it is widely used to evaluate the performance of different types of the modulation scheme of UWA communication. The watermark channel uses the equation below to evaluate the performance of the system.

$$y(t) = \int_{-\infty}^{\infty} \hat{h}(t, \tau) x(t - \tau) d\tau + n(t) \tag{19}$$

where $y(t)$ is the output of the time-varying UWA channel recorded impulse response $\hat{h}(t, \tau)$ of the real channel $h(t, \tau)$, while $x(t)$ is the input signal and $n(t)$ is the noise. The watermark offers many different types of channels. The channel used in this simulation is NOF1 (Norway Oslofjord). The details of the simulation parameters are shown in

Fig. 17 BER versus SNR graph proposed system in watermark channel **a** BER versus SNR graph of HCS Chirp, FCS Chirp and LFM with SF 9sHz and 8.65, respectively, and Chirp Period 5 ms, **b** BER versus SNR graph of HCS Chirp, FCS chirp and LFM with SF 4.4sHz and 5.5, respectively, and Chirp Period 5 ms
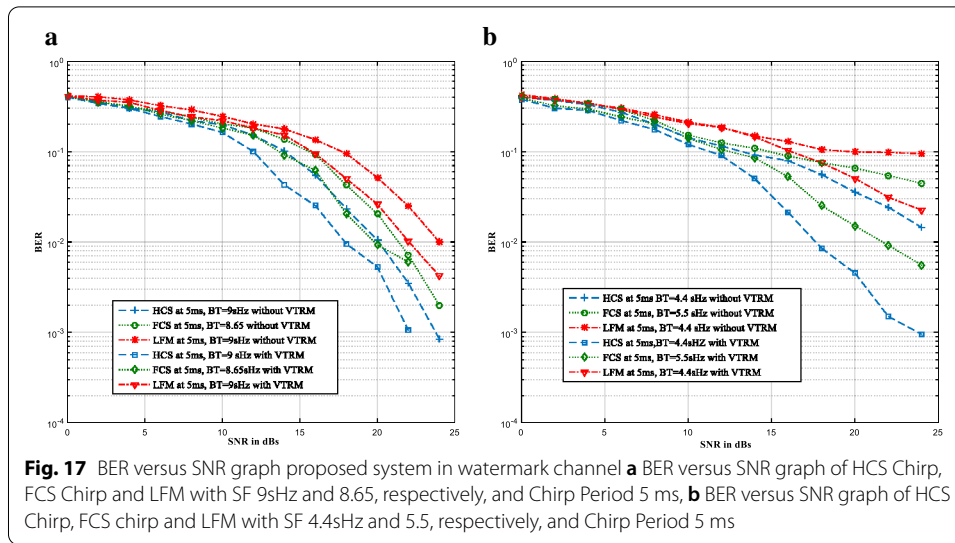
Table 2. It is to be noted that both the transmitter and receiver are static and time-varying Doppler is compensated using resampling. The impulse response of the channel is shown in Fig. 15. The performance of the HCS and LFM chirp was evaluated at BT 9sHz and 4.4sHz, while the performance of FCS at 8.65 sHz and 5.5 sHz. The results in Fig. 16 shows that the performance of both the nonlinear chirps are better than the linear chirp, but NOF1 channel requires higher SNR to achieve satisfactory performance compared to the BELLHOP channel. In addition, VTRM is used to improve the performance of the system. Moreover, the performance of the linear and nonlinear chirp is also evaluated at 5 ms and SF 9 sHz for HCS and LFM and 8.65 sHz for FCS in NOF1 channel. The results show that linear chirp performance is acceptable after 18 dBs at BT = 9sHz and improves after VTRM processing while the performance of HCS and FCS at 5 ms remains superior then LFM and further improves after using VTRM as shown in Fig. 17a. Furthermore, when the BT of the LFM and HCS was decreased to 4.4sHz, and for FCS 5.5sHz, the LFM showed disappointing results, on the other hand performance of both the nonlinear chirp also degraded, however after VTRM processing the nonlinear chirp showed satisfactory results, while HCS was better than FCS as shown in Fig. 17b.

8 Conclusion and future work

In this paper, MS-CSS-VTRM is proposed. The mentioned technique uses nonlinear Sine chirp, which can perform better at low spreading factor, which plays a significant role in hydro-acoustic communication's overall performance. However, to increase the information rate, M-ary technique is presented by transmitting the chirp at different frequency bands. At the same time, VTRM equalizes the UWA channel to minimize the effect of multipath interference. As a result, the overall reliability of the system is improved. Firstly, the paper presented the sine chirp and proved that at low SF it is orthogonal. Secondly, the system model of the M-ary sine chirp spread spectrum is presented. Then, the concept of VTRM in underwater acoustic communication to mitigate inter-symbol interference is presented. Finally, the MS-CSS scheme proposed in this

Liu *et al. J Wireless Com Network*   (2021) 2021:112

Page 18 of 20

article is compared to traditional linear chirp. The simulation results proved that the proposed scheme is robust to the multipath environment and performed better than the conventional linear chirp system. In future work, we will perform sea trials to analyze the proposed scheme's performance in the real-world underwater acoustic channel. The time variability due to water surface movements, tides, internal waves, and Doppler shift caused by moving devices such as AUVs will also be analyzed.

Abbreviations
AUV: Autonomous underwater vehicle; LFM: Linear frequency modulation; CDMA: Code-division multiple access; FDMA: Frequency-division spread spectrum; VTRM: Virtual time-reversal mirror method; SF: Spread factor; BT: Bandwidth time; LoRA: Low-power long-range wide area network; BOK: Binary orthogonal keying; DM: Direct modulation; MU-CSS: M-ary sine chirp spread spectrum; MP: Matching pursuit; HCS: Half cycle sine; FCS: Full cycle sine; BER: Bit error rate; UWA: Underwater acoustic; AWGN: Additive white Gaussian noise; UWSNs: Underwater wireless sensor networks.

Authors' contributions
All the authors contributed in the preparation of this manuscript, following are the detail of the contributions Conceptualization, S.L. and H.Z.; methodology, S.L. and H.Z.; software, H.Z.; validation, S.L., L.Y. and M.B; formal analysis, S.L., H.Z. and L.Y; investigation, H.Z.,S.L and L.Y; resources, S.L.; data curation, S.L.,S.S. and WR.; writing—original draft preparation, H.Z.; writing—review and editing, S.L.,L.Y. and M.B.; visualization, S.L. and H.Z; supervision, S.L.; project administration, S.L. All authors read and approved the final manuscript.

Availability of data and materials
Not applicable.

Declarations

Competing interest
The authors declare no competing interest.

Author details
[1]Acoustic Science and Technology Laboratory, Harbin Engineering University, Harbin 150001, China. [2]Key Laboratory of Marine Information Acquisition and Security, Harbin Engineering University, Ministry of Industry and Information Technology, Harbin 150001, China. [3]College of Underwater Acoustic Engineering, Harbin Engineering University, Harbin 150001, China.

References

1. O. Gupta, N. Goyal, The evolution of data gathering static and mobility models in underwater wireless sensor networks: a survey. J. Ambient Intell. Humaniz. Comput. (2021). https://doi.org/10.1007/s12652-020-02719-z
2. N. Goyal, M. Dave, A.K. Verma, SAPDA: secure authentication with protected data aggregation scheme for improving QoS in scalable and survivable UWSNs. Wirel. Pers. Commun. **113**, 1–15 (2020)
3. M. Stojanovic, J. Preisig, Underwater acoustic communication channels: propagation models and statistical characterization. IEEE Commun. Mag. **47**(1), 84–89 (2009). https://doi.org/10.1109/mcom.2009.4752682
4. M. Choudhary, N. Goyal, Routing protocol design issues and challenges in underwater wireless sensor network, in *Energy-Efficient Underwater Wireless Communications and Networking* (IGI Global, 2021), pp. 1–15
5. L. Freitag et al., Analysis of channel effects on direct-sequence and frequency-hopped spread-spectrum acoustic communication. IEEE J. Oceanic Eng. **26**(4), 586–593 (2001). https://doi.org/10.1109/48.972098
6. M.R. Winkler, Chirp signals for communications. WESCON Convention Record, 1962. Paper 14.2
7. B. Reynders, S. Pollin, Chirp spread spectrum as a modulation technique for long range communication, in *2016 Symposium on Communications and Vehicular Technologies (SCVT)* (IEEE, 2016). https://doi.org/10.1109/SCVT.2016.7797659

Liu *et al. J Wireless Com Network*   (2021) 2021:112

Page 19 of 20

8. T.T. Nguyen et al., Efficient design of chirp spread spectrum modulation for low-power wide-area networks. IEEE Internet Things J. **6**(6), 9503–9515 (2019)
9. M. Palmese, et al. Experimental validation of a chirp-based underwater acoustic communication method. In *Proceedings of Meetings on Acoustics 155ASA*. (Acoustical Society of America, 2008). https://doi.org/10.1121/1.2988054
10. F. Steinmetz, J. Heitmann, C. Renner. A practical guide to chirp spread spectrum for acoustic underwater communication in shallow waters, in *Proceedings of the Thirteenth ACM International Conference on Underwater Networks & Systems* (2018). https://doi.org/10.1145/3291940.3291964
11. X. Wang, M. Fei, X. Li, Performance of chirp spread spectrum in wireless communication systems, in *2008 11th IEEE Singapore International Conference on Communication Systems* (IEEE, Singapore, 2008). https://doi.org/10.1109/ICCS.2008.4737227
12. K. Kebkal, A. Kebkal, S. Yakovlev, A frequency-modulated-carrier digital communication technique for multipath underwater acoustic channels. Acoust. Phys. **50**(2), 177–184 (2004). https://doi.org/10.1134/1.1675873
13. K. Kebkal, R. Bannasch, A. Kebkal, Estimation of phase error limits for PSK-modulated sweep-spread carrier signal, in *Oceans' 04 MTS/IEEE Techno-Ocean'04 (IEEE Cat. No. 04CH37600)* (IEEE, 2004). https://doi.org/10.1109/OCEANS.2004.1405536
14. N. Levanon, *Principles Radar* (Wiley, New York, 1988).
15. A.W. Doerry, *Generating Nonlinear FM Chirp Waveforms for Radar* (Sandia National Laboratories, Albuquerque, 2006).
16. T. Collins, P. Atkins, Nonlinear frequency modulation chirps for active sonar. IEE Proc. Radar Sonar Navig. **146**(6), 312–316 (1999). https://doi.org/10.1049/ip-rsn:19990754
17. M.A. Khan, R.K. Rao, X. Wang, Performance of quadratic and exponential multiuser chirp spread spectrum communication systems, in *2013 International Symposium on Performance Evaluation of Computer and Telecommunication Systems (SPECTS)* (IEEE, 2013)
18. C. Bernard et al., Multiuser chirp spread spectrum transmission in an underwater acoustic channel applied to an AUV fleet. Sensors **20**(5), 1527 (2020). https://doi.org/10.3390/s20051527
19. M.O. Khyam et al., Multiple access chirp-based ultrasonic positioning. IEEE Trans. Instrum. Meas. **66**(12), 3126–3137 (2017)
20. Z. Sun et al., Parameter estimation technique for the SNCK scheme based on the spectral-correlation density. Wirel. Pers. Commun. **82**(3), 1505–1529 (2015)
21. Z. Sun, X. Ning, D. Tian, Time-frequency bandwidth product estimation of Sinusoidal Non-linear Chirp Keying scheme. China Commun. **14**(8), 184–194 (2017)
22. Q. Wang, J. Jiang, Performances of trigonometric chirp spread spectrum modulation in AWGN & Rayleigh channels, in *Proceedings of the 8th ACM Workshop on Performance Monitoring and Measurement of Heterogeneous Wireless and Wired Networks* (2013). https://doi.org/10.1145/2512840.2512869
23. Z.-G. Sun et al., Approach to sine non-linear chirp keying modulation and performance analysis. Syst. Eng. Electron. **35**(2), 414–419 (2013)
24. M. Alsharef, R.K. Rao, M-ary chirp modulation for coherent and non-coherent data transmission, in *IEEE 28th Canadian Conference on Electrical and Computer Engineering (CCECE)* (IEEE, Halifax, Canada), pp. 213–219
25. C. He, M.R.Q. Meng, J. Huang, Underwater acoustic communications using M-ary chirp-DPSK modulation, in *IEEE 10th International Conference on Signal Processing Proceedings* (Beijing, 2010), pp. 1544–1547
26. F. Zhou et al., M-ary cyclic shift keying spread spectrum underwater acoustic communications based on virtual time-reversal mirror. Sensors **19**(16), 3577 (2019). https://doi.org/10.3390/s19163577
27. J. Huang, C. He, Q. Zhang, M-ary chirp spread spectrum modulation for underwater acoustic communication, in *TENCON 2005–2005 IEEE Region 10 Conference* (IEEE, 2005). https://doi.org/10.1109/TENCON.2005.301178
28. C.E. Cook, Pulse compression-key to more efficient radar transmission. Proc. IRE **48**(3), 310–316 (1960)
29. A. Springer et al., A wireless spread-spectrum communication system using SAW chirped delay lines. IEEE Trans. Microw. Theory Tech. **49**(4), 754–760 (2001). https://doi.org/10.1109/22.915460
30. Q. Wang, Non-linear chirp spread spectrum communication systems of binary orthogonal keying mode, in *Electrical and Computer Engineering* (The University of Western Ontario, 2015)
31. C.R. Berger et al., Application of compressive sensing to sparse channel estimation. IEEE Commun. Mag. **48**(11), 164–174 (2010)
32. L. Liu et al., Modelling and simulation of pseudo-noise sequence-based underwater acoustic OSDM communication system. Appl. Sci. **9**(10), 2063 (2019)
33. S.F.C.A.B.D. Rao, Sparse channel estimation via matching pursuit with application to equalization. IEEE Trans. Commun. **50**(3), 374–377 (2002). https://doi.org/10.1109/26.990897
34. S. Liu, et al., Covert underwater acoustic communication using whale noise masking on DSSS signal, in *2013 MTS/IEEE OCEANS-Bergen* (IEEE, 2013)
35. M. Bilal et al., Bionic Morse coding mimicking humpback whale song for covert underwater communication. Appl. Sci. **10**(1), 186 (2020)
36. S. Jesus, A. Silva, Virtual time-reversal in underwater communications. Results on the INTIFANTE'00 Sea trial, in *Forum Acusticum 2002*. 2002.
37. F. Yuan, Q. Wei, E. Cheng, Joint virtual time reversal communications with an orthogonal chirp spread spectrum over underwater acoustic channel. Appl. Acoust. **117**, 122–131 (2017)
38. F. Yuan, Q. Wei, E. Cheng, Multiuser chirp modulation for underwater acoustic channel based on VTRM. Int. J. Nav. Archit. Ocean Eng. **9**(3), 256–265 (2017)

39. Y. Luan, et al., Doppler estimation using time reversal mirror for underwater acoustic time-varying multipath channel, in *2017 IEEE International Conference on Signal Processing, Communications and Computing (ICSPCC)* (IEEE, 2017)
40. A. Zhao et al., An underwater time reversal communication method using symbol-based Doppler compensation with a single sound pressure sensor. Sensors **18**(10), 3279 (2018)
41. A. Silva, S. Jesus, Underwater communications using virtual time reversal in a variable geometry channel, in *OCEANS'02 MTS/IEEE* (IEEE, 2002). https://doi.org/10.1109/OCEANS.2002.1192005
42. L. Wen-cong, et al., Underwater acoustic communication based on virtual time reversal and sweep-spread carrier, in *OCEANS 2016-Shanghai* (IEEE, 2016). https://doi.org/10.1109/OCEANSAP.2016.7485563
43. P. van Walree, A.R. Otnes, T. Jenserud, Watermark: a realistic benchmark for underwater acoustic modems, in *IEEE Third Underwater Communications and Networking Conference (UComms)* (IEEE, Lerici, 2016), pp. 1–4

Publisher's Note